Drift-Diffusion Simulation for Quantitative Interpretation of STEM-EBIC on FIB-Prepared Silicon p-n Junctions

Chenyang Yu[1,*], Sebastian Schneider[2], Bernd Rellinghaus[2], and Christoph Jungemann[1]
[1]Institute of Electromagnetic Theory, RWTH Aachen University, Aachen, Germany
[2]Dresden Center for Nanoanalysis (DCN), cfaed, TUD Dresden University of Technology, Dresden, Germany

***Abstract*—Scanning transmission electron microscopy beam-induced current (STEM-EBIC) offers nanoscale mapping of carrier collection in FIB-prepared semiconductor lamellae. However, quantitative interpretation is challenging because the measured current is influenced by internal electric fields, carrier diffusion, exposed surfaces, finite lamella geometry, and contact boundary conditions. In this work, we use two-dimensional drift-diffusion simulations of the experimental lamella geometry to interpret STEM-EBIC measurements on a FIB-prepared silicon p–n junction. The simulations show that the experimentally observed sub-micrometer apparent collection lengths are not reproduced by realistic bulk Shockley–Read–Hall recombination alone. Instead, the profile width and its thickness dependence are mainly controlled by recombination at the exposed lamella surfaces, with an effective surface recombination velocity on the order of $10^6\,\mathrm{cm/s}$. A separate surface-charge analysis identifies the regime in which charged surface states can deplete thin or lightly doped lamellae. These results indicate that STEM-EBIC line scans in FIB-prepared lamellae should be interpreted as surface-limited effective collection profiles rather than direct bulk diffusion-length measurements, and provide practical guidance for assessing when measured profiles remain representative of the underlying junction.**

***Index Terms*—STEM-EBIC, drift-diffusion simulation, FIB lamella, Si p-n junction, surface recombination, Schottky contact**

I. Introduction

Scanning transmission electron microscopy beam-induced current (STEM-EBIC) imaging offers nanoscale spatial resolution for mapping charge carrier behavior in semiconductor devices. In EBIC, a focused electron beam generates electron–hole pairs in the sample, which are separated by internal electric fields and collected as a current at external contacts [1], providing a spatially resolved map of carrier collection efficiency. Unlike conventional SEM-EBIC, which operates on bulk samples with interaction volumes limited by beam energy and carrier diffusion, STEM-EBIC works with thin FIB-prepared lamellae where the beam is mostly transmitted and carrier generation is confined primarily along the beam path [2]. This has enabled STEM-EBIC to emerge as a powerful characterization technique with demonstrated resolution down to the angstrom scale [3], but the thin-lamella geometry also makes the measured signal highly sensitive to boundary conditions introduced during sample preparation.

This research was funded by the Deutsche Forschungsgemeinschaft (DFG) within TRR 404 Active-3D (project number 528378584).

Recent experimental work has demonstrated both the promise and the difficulty of quantitative STEM-EBIC analysis. Schneider et al. [4] reported systematic STEM-EBIC measurements on FIB-prepared silicon photodiode lamellae, extracting effective diffusion lengths orders of magnitude below typical bulk-Si values and observing a clear dependence of both peak current and profile width on lamella thickness. Moynihan et al. [5] combined in-operando 4D-STEM and STEM-EBIC on biased silicon p–n junctions and showed that the EBIC signal does not directly follow the electric-field distribution alone, but is also shaped by carrier diffusion and recombination. These studies motivate simulations that retain the finite lamella geometry and explicitly account for the exposed FIB-prepared surfaces.

In this work, the STEM-EBIC measurements of Schneider et al. [4] are interpreted using two-dimensional drift-diffusion simulations of the corresponding FIB-prepared silicon p–n junction lamella. The simulation domain is constructed from the measured lamella geometry and explicitly includes the exposed top and bottom surfaces, allowing the individual roles of recombination, contacts, and surface charge to be isolated. This approach is used to determine which mechanisms control the measured peak current, profile width, thickness dependence, and extracted apparent diffusion length.

II. Experiment and Device

The device under study is a commercial silicon photodiode with a p–n junction located approximately $1.5\,\mu\mathrm{m}$ below the surface. A TEM lamella was prepared by focused ion beam milling, mounted with tungsten on a MEMS chip with platinum contacts, and further thinned by low-energy argon ion milling to remove amorphous damage layers [4]. The lamella has lateral dimensions of approximately $14\,\mu\mathrm{m} \times 8.5\,\mu\mathrm{m}$ and features an asymmetric slit geometry that defines the current collection path. The slits cut through the junction and isolate the n- and p-type regions, providing separate electrical access to each side (Fig. 1).

STEM-EBIC measurements were performed at $200\,\mathrm{keV}$ with a beam current of approximately $82.5\,\mathrm{pA}$. At this energy, nearly all electrons are transmitted through the thin lamella with negligible backscattering [2], so that the electron–hole pair generation can be approximated as uniform along the beam path. Measurements were carried out across lamella

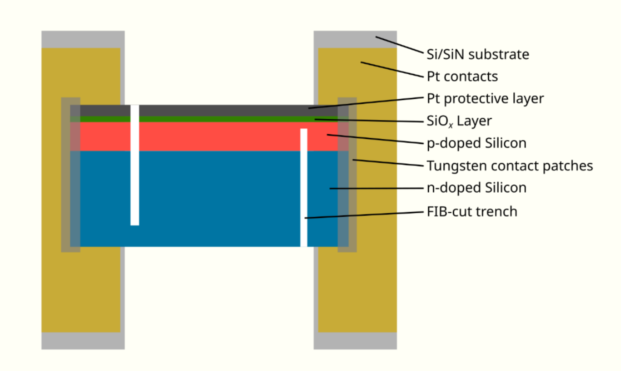

Fig. 1. Top view of the FIB-prepared lamella showing the contact layout and slit geometry [4].

thicknesses ranging from 127 to 530 nm [4]. The data reveal a systematic thickness dependence of both the peak EBIC current and the effective diffusion length L_{eff}, as well as preparation-induced artifacts from FIB-damaged amorphous surface layers that progressively disappear after argon milling [4]. The extracted L_{eff} values are 0.2–0.4 µm, indicating strongly shortened apparent collection profiles in the FIB-prepared lamella.

The doping profile of the commercial photodiode is not independently available. However, the EBIC line shape provides constraints on the junction electrostatics, since the apparent depletion width and the relative decay lengths on the p- and n-type sides depend on the local doping levels. We therefore use an effective p–n junction profile with approximately symmetric doping, choosing a nominal concentration of order $10^{17}\,\mathrm{cm}^{-3}$ to reproduce the observed depletion-region width and the measured L_p/L_n ratio. This effective profile is then used for the quantitative comparisons in Section IV.

III. Simulation Framework

The EBIC experiment is modeled within the drift-diffusion framework, solving Poisson's equation together with the electron and hole continuity equations using a finite volume method. Carrier current densities are discretized using the Scharfetter–Gummel scheme [6], and the resulting nonlinear system is solved with a fully coupled Newton–Raphson method. All simulations are performed using an in-house drift-diffusion simulator.

To account for the exposed FIB-prepared surfaces, the simulation domain is chosen as a two-dimensional cross-section of approximately $5\,\mu\mathrm{m} \times t$, containing both the beam direction and the EBIC scan direction, where t is the lamella thickness (Fig. 2). In this geometry, the top and bottom surfaces are explicitly resolved as simulation boundaries, so that surface recombination and, in the charged-trap analysis, surface charge can be included directly in the model. The junction position and contact layout follow the experimental geometry, while the nominal doping profile follows the estimate described in Section II. In the silicon region, bulk recombination is described by the standard Shockley–Read–Hall (SRH) model [7], [8] with midgap traps and doping-dependent lifetimes according to the Scharfetter relation [9]. At the FIB-prepared surfaces, recombination is described by an SRH-type boundary condition with effective surface recombination velocity S. This parameter is varied to assess how recombination at the exposed lamella surfaces affects the EBIC current and the extracted L_{eff}. In the charged-trap analysis, the surface traps also carry charge determined by their occupation, and this charge is included self-consistently in Poisson's equation. The metal–semiconductor interfaces are treated as Schottky contacts. The carrier fluxes at these boundaries are described using a thermionic-emission contact model [10] with literature barrier heights for the W–Si interfaces; tunneling and image-force barrier lowering are neglected.

Electron-beam excitation is modeled by a position-dependent generation term distributed along the transmitted beam path and over the prescribed beam cross-section. The generation distribution extends through the lamella thickness, while its magnitude is set by the beam current and the electron stopping power in silicon at the experimental beam energy [11]. A full EBIC line profile is obtained by sweeping the generation source across the domain and recording the terminal current at each beam position.

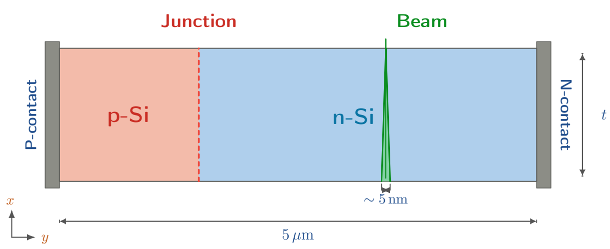

Fig. 2. Cross-sectional simulation domain used for the two-dimensional drift-diffusion model. The domain contains both the beam direction and the EBIC scan direction, resolves the top and bottom FIB-prepared surfaces, and includes the estimated p–n junction doping profile and contact geometry used in the experimental comparison.

IV. Results and Interpretation

A. Bulk recombination has limited influence under realistic conditions

In thin FIB-prepared lamellae, the large surface-to-volume ratio raises the question of whether bulk or surface recombination limits the effective diffusion length. The bulk contribution is first isolated by disabling surface recombination and sweeping the SRH lifetime over realistic and intentionally extreme values (Fig. 3). For realistic carrier lifetimes, bulk SRH recombination has negligible influence on the profile width, with visible narrowing appearing only for unrealistically short, picosecond-scale lifetimes. Thus, for the geometry and estimated doping profile used in the experimental comparison, bulk SRH recombination alone does not reproduce the measured short L_{eff} range. This motivates a separate assessment of recombination at the exposed lamella surfaces.

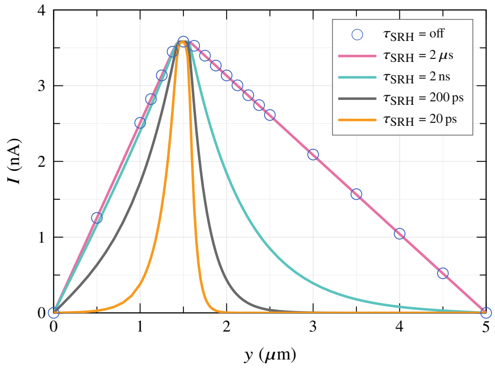

Fig. 3. Simulated EBIC profiles from the bulk-lifetime sweep with surface recombination disabled. The lifetime range spans $\tau_n = 2\,\mu\text{s}$, $\tau_p = 0.5\,\mu\text{s}$, corresponding to $N_{\text{dop}} = 10^{17}\,\text{cm}^{-3}$ via the Scharfetter relation, down to $\tau_n = 20\,\text{ps}$, $\tau_p = 5\,\text{ps}$.

B. Surface recombination velocity controls L_{eff} and peak current

With bulk SRH ruled out as the dominant loss mechanism, the surface recombination velocity S is varied within the same geometry. Simulations are performed at fixed lamella thickness with S varied from 10^5 to 10^7 cm/s (Fig. 4). Increasing S reduces the peak EBIC current and shortens L_{eff} on both sides of the junction, resulting in narrower EBIC profiles. This narrowing is more clearly visible after normalization, indicating that S controls not only the signal amplitude but also the spatial extent over which carriers are collected. Comparison with the experimental L_{eff} range indicates an effective surface recombination velocity on the order of 10^6 cm/s for the Ar-milled lamella surfaces [4].

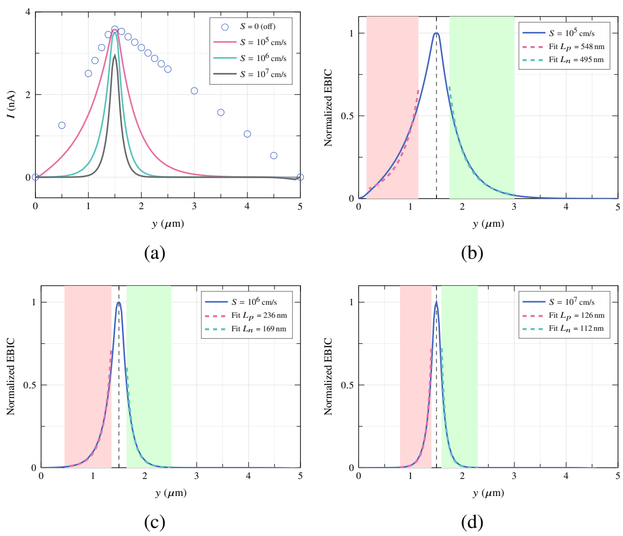

Fig. 4. (a) Simulated EBIC profiles for surface recombination velocities $S = 10^5$, 10^6, and 10^7 cm/s, showing the reduction in peak current and profile narrowing with increasing S. (b)–(d) Normalized profiles for each S value with the fitting regions for L_{eff} extraction indicated on the p-side (red) and n-side (green). Fits follow $I(x) = k\,x^{-1/2}\exp(-x/L_{\text{eff}})$ [12], assuming strong surface recombination ($\alpha = -1/2$).

C. Thickness dependence reproduces experimental trend

Using the surface recombination velocity identified from the L_{eff} comparison in Fig. 4, the lamella thickness is varied from $t = 400\,\text{nm}$ down to $250\,\text{nm}$ while all other parameters are kept fixed (Fig. 5). Reducing the thickness lowers the peak EBIC current and shortens the extracted L_{eff}, in agreement with the experimentally observed thickness dependence. The thickness dependence can be understood from two contributions. First, for a transmitted beam, a thinner lamella provides a shorter generation path through silicon and therefore produces fewer electron–hole pairs per incident electron. Second, the surface-to-volume ratio increases as the lamella thins, so that a larger fraction of the generated carriers is lost to surface recombination before reaching the junction. The reduced generation mainly lowers the absolute signal, whereas enhanced surface recombination also narrows the collection profile. With a single fixed surface recombination velocity, the simulations capture the main thickness-dependent trends, supporting a surface-limited interpretation of the measured EBIC profiles.

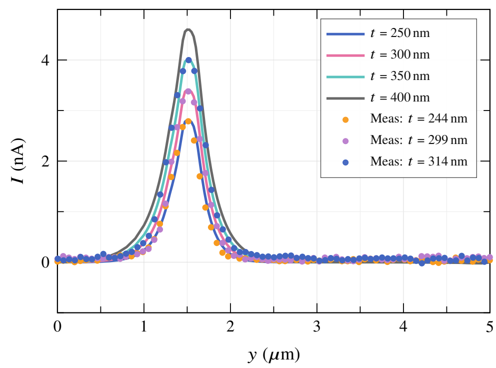

Fig. 5. Simulated absolute EBIC profiles for lamella thicknesses from $t = 400\,\text{nm}$ down to $250\,\text{nm}$ at fixed surface recombination velocity. Measured profiles (markers) are shifted to align the peak position and normalized to the simulated peak current for shape comparison. The thickness sweep is used to compare the simulated and measured profile shapes at fixed S.

V. Surface-Charge Validity Limit for Thin and Lightly Doped Lamellae

The top and bottom lamella surfaces have so far been treated as electrically neutral recombination sinks characterized by an effective surface recombination velocity S. However, surface states can also carry charge and thereby modify the electrostatic potential inside the lamella. Following Haney et al. [13], the trap occupation is computed from the local carrier concentrations, and the resulting sheet charge is included self-consistently in Poisson's equation. Under the midgap charge convention used here, traps are mostly electron-occupied and negatively charged in n-type regions, while the opposite sign occurs in p-type regions. In thin or lightly doped lamellae, depletion regions induced by the two charged surfaces can overlap, reshaping the junction field and suppressing EBIC collection. This mechanism may contribute to the strong signal loss reported after extreme lamella thinning [14].

The onset of surface-induced full depletion can be estimated from a simple charge-balance argument. Here, N_{surf} denotes the surface-state density per exposed surface. With the charged-trap convention used here [13], the sheet charge density at each surface is $\rho_{\mathrm{surf}} = qN_{\mathrm{surf}}(1-2f_{\mathrm{surf}})/2$, where f_{surf} is the electron occupation probability of the surface trap state, so that the effective charged sheet density in the strongly charged limit is approximately $N_{\mathrm{surf}}/2$ per surface. Balancing this sheet charge with the ionized dopant charge gives a characteristic depletion width $W_{\mathrm{surf}} \approx N_{\mathrm{surf}}/(2N_{\mathrm{dop}})$, where N_{dop} is the local dopant concentration. Since depletion can extend inward from both exposed surfaces, overlap occurs when $2W_{\mathrm{surf}} \approx t$, yielding the order-of-magnitude criterion $N_{\mathrm{surf,crit}} \approx N_{\mathrm{dop}}t$.

Charged-surface effects are therefore expected to become important as $\chi = N_{\mathrm{surf}}/(N_{\mathrm{dop}}t)$ approaches unity. For the reference device, $N_{\mathrm{dop}} \approx 10^{17}\,\mathrm{cm}^{-3}$ and $t \approx 300\,\mathrm{nm}$ give $N_{\mathrm{dop}}t \approx 3 \times 10^{12}\,\mathrm{cm}^{-2}$, making surface-induced depletion unlikely to dominate the measured EBIC profiles. To illustrate the surface-charge-sensitive regime, a lower-doped symmetric junction with $N_{\mathrm{dop}} = 10^{15}\,\mathrm{cm}^{-3}$ and $t = 300\,\mathrm{nm}$ is simulated, for which $N_{\mathrm{surf,crit}} \approx 3 \times 10^{10}\,\mathrm{cm}^{-2}$. As shown in Fig. 6, $N_{\mathrm{surf}} = 10^{10}\,\mathrm{cm}^{-2}$ remains close to the neutral-surface result, whereas $N_{\mathrm{surf}} = 10^{11}\,\mathrm{cm}^{-2}$ reduces the peak current by roughly two orders of magnitude.

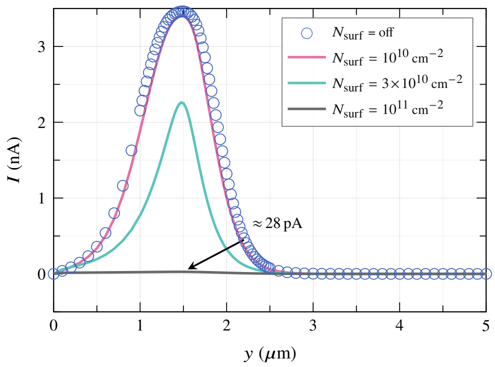

Fig. 6. Simulated absolute EBIC profiles for the lightly doped test case ($N_{\mathrm{dop}} = 10^{15}\,\mathrm{cm}^{-3}$, $t = 300\,\mathrm{nm}$) as the effective charged surface-state density N_{surf} per exposed surface is varied.

These results define a validity condition for quantitative STEM-EBIC interpretation. For $\chi = N_{\mathrm{surf}}/(N_{\mathrm{dop}}t) \ll 1$, surface charge acts only as a perturbation, and the neutral-surface recombination model can remain adequate. As χ approaches unity, surface-induced depletion can span the lamella, reshape the junction field, and strongly suppress carrier collection; in this regime, EBIC profiles should be interpreted with explicit surface-charge modeling. Thus, increasing lamella thickness, increasing doping, or reducing the charged surface-state density moves the sample away from the surface-charge-depleted regime and provides a practical criterion for preparing and interpreting FIB lamellae for quantitative STEM-EBIC.

VI. Conclusion

Two-dimensional drift-diffusion simulations were used to analyze STEM-EBIC line profiles from a FIB-prepared silicon p–n junction lamella. Within the estimated doping profile and experimental lamella geometry, the profile width, peak current, and their thickness dependence are primarily controlled by recombination at the exposed lamella surfaces. The measured profiles are therefore best interpreted as surface-limited effective collection profiles rather than direct measurements of the bulk diffusion length.

The charged-surface analysis further shows that surface charge must be considered when the charged surface-state density becomes comparable to the dopant charge contained within the lamella thickness. In thin or lightly doped lamellae, surface-induced depletion can reshape the junction electrostatics and strongly suppress the EBIC signal. Therefore, quantitative STEM-EBIC on FIB-prepared lamellae requires treating the exposed surfaces as active electrical boundaries rather than passive geometric truncations of the original device.

References

[1] C. Donolato, "Theory of beam induced current characterization of grain boundaries in polycrystalline solar cells," *Journal of Applied Physics*, vol. 54, no. 3, pp. 1314–1322, 1983.

[2] A. P. Conlan, G. Moldovan, L. Bruas, E. Monroy, and D. Cooper, "Electron beam induced current microscopy of silicon p-n junctions in a scanning transmission electron microscope," *Journal of Applied Physics*, vol. 129, no. 13, p. 135701, 2021.

[3] M. Mecklenburg, W. A. Hubbard, J. J. Lodico, and B. C. Regan, "Electron beam-induced current imaging with two-angstrom resolution," *Ultramicroscopy*, vol. 207, p. 112852, 2019.

[4] S. Schneider, S. Beckert, R. Hammer, M. König, G. Moldovan, and D. Pohl, "STEM EBIC as a quantitative probe of semiconductor devices," arXiv:2511.11528, 2025.

[5] E. Moynihan, Y. Xie, D. Cooper, G. Moldovan, R. Beanland, and A. Sanchez, "In-operando 4D-STEM and STEM-EBIC imaging of electric fields and charge carrier behavior in biased silicon p–n junctions," *Advanced Electronic Materials*, vol. 12, no. 5, p. e00415, 2026.

[6] D. L. Scharfetter and H. K. Gummel, "Large-signal analysis of a silicon Read diode oscillator," *IEEE Transactions on Electron Devices*, vol. 16, no. 1, pp. 64–77, 1969.

[7] W. Shockley and W. T. Read, "Statistics of the recombinations of holes and electrons," *Physical Review*, vol. 87, no. 5, pp. 835–842, 1952.

[8] R. N. Hall, "Electron-hole recombination in germanium," *Physical Review*, vol. 87, no. 2, p. 387, 1952.

[9] *Sentaurus Device User Guide*, Synopsys, Inc., Mountain View, CA, 2023.

[10] S. M. Sze, Y. Li, and K. K. Ng, *Physics of Semiconductor Devices*. John Wiley & Sons, 2021.

[11] M. J. Berger, J. S. Coursey, and M. A. Zucker, "ESTAR, PSTAR, and ASTAR: Computer programs for calculating stopping-power and range tables for electrons, protons, and helium ions," NIST Standard Reference Database 124, version 1.21, 1999, updated February 17, 2017.

[12] V. K. S. Ong, J. C. H. Phang, and D. S. H. Chan, "A direct and accurate method for the extraction of diffusion length and surface recombination velocity from an EBIC line scan," *Solid-State Electronics*, vol. 37, no. 1, pp. 1–7, 1994.

[13] P. M. Haney, H. P. Yoon, B. Gaury, and N. B. Zhitenev, "Depletion region surface effects in electron beam induced current measurements," *Journal of Applied Physics*, vol. 120, no. 9, p. 095702, 2016.

[14] S. Schneider, D. Pohl, and B. Rellinghaus, "Perspectives and limitations of STEM EBIC measurements for the characterization of semiconductor devices," *Microscopy and Microanalysis*, vol. 31, no. 7, pp. 1743–1744, 2025.